ELSEVIER

Available online at www.sciencedirect.com

SCIENCE DIRECT®

Tectonophysics 412 (2006) 183–193

TECTONOPHYSICS

www.elsevier.com/locate/tecto

Mesozoic–Tertiary exhumation history of the Altai Mountains, northern Xinjiang, China: New constraints from apatite fission track data

Wanming Yuan [a,]*, Andy Carter [b], Jinquan Dong [a], Zengkuan Bao [a], Yinchang An [c], Zhaojie Guo [d]

[a] *Laboratory of Nuclear analysis techniques, Institute of High Energy Physics, Chinese Academy of Sciences, Beijing, 100039, China*
[b] *Research School of Earth Sciences, University and Birkbeck College, London WC1E 6BT, United Kingdom*
[c] *Institute of Exploration of Nonferrous Metal Geology and Mineral Resources, Xinjiang Uygur Autonomous Region, Urumchi 830000, China*
[d] *Department of Geology, Peking University, Beijing, 100871, China*

Received 20 February 2005; received in revised form 5 August 2005; accepted 28 September 2005
Available online 1 December 2005

Abstract

This study uses apatite fission track (FT) analysis to constrain the exhumation history of bedrock samples collected from the Altai Mountains in northern Xinjiang, China. Samples were collected as transects across the main structures related to Palaeozoic crustal accretion events. FT results and modeling identify three stages in sample cooling history spanning the Mesozoic and Tertiary. Stage one records rapid cooling to the low temperature part of the fission track partial annealing zone circa 70 ± 10 °C. Stage two, records a period of relative stability with little if any cooling taking place between ~75 and ~25–20 Ma suggesting the Altai region had been reduced to an area of low relief. Support for this can be found in the adjacent Junngar Basin that received little if any sediment during this interval. Final stage cooling took place in the Miocene at an accelerated rate bringing the sampled rocks to the Earth's surface. This last stage, linked to the far field effects of the Himalayan collision, most likely generated the surface uplift and relief that define the present-day Altai Mountains.

Keywords: Apatite fission track; Tectonics; Uplift; Topography; Erosion; Altai Mountains

1. Introduction

The 2000 km long southeast–northwest trending Altai Mountains of central Asia extend from the Gobi desert in the east to the Siberian Plain in the west. The rocks that outcrop in the present-day mountains have a long and complex history involving several periods of tectonism and uplift that extend back into the Late Precambrian. The origin of the mountains as we known them today is unclear. A paucity of exhumation data means little is known about how the Altai Mountains evolved throughout the Mesozoic and Cenozoic. Are the mountains a long-lived feature or a more recent development, perhaps linked to the India–Eurasia collision?

The most important event in the history of the Altai region can be traced back to the Palaeozoic when a series of terrane accretion–subduction events associated with the Kazakhstan-Junggar plates and Siberian

---

* Corresponding author. Fax: +86 10 88233186.
E-mail address: yuanwm@mail.ihep.ac.cn (W. Yuan).

0040-1951/$ - see front matter © 2005 Elsevier B.V. All rights reserved.
doi:10.1016/j.tecto.2005.09.007

Craton produced an orogen alongside the slightly older and much larger Sayan-Mongolian fold belt. Subduction of the Karakhstan-Junggar plate northwards along the Irtysch fault zone began in the early Paleozoic with emplacement of subduction related plutons accompanied by folding and thrusting that gradually transferred and intensified from the north-east to south-west (Chen et al., 1997; Wang and Cheng, 2001). Whether these early accretion–collision events generated a large mountain belt is unclear however there is a general consensus that by the early Mesozoic the Altai region had become a significant topographic feature as evidenced by significant thickness of continental deposits in the adjacent Junggar Basin of northern Xinjiang.

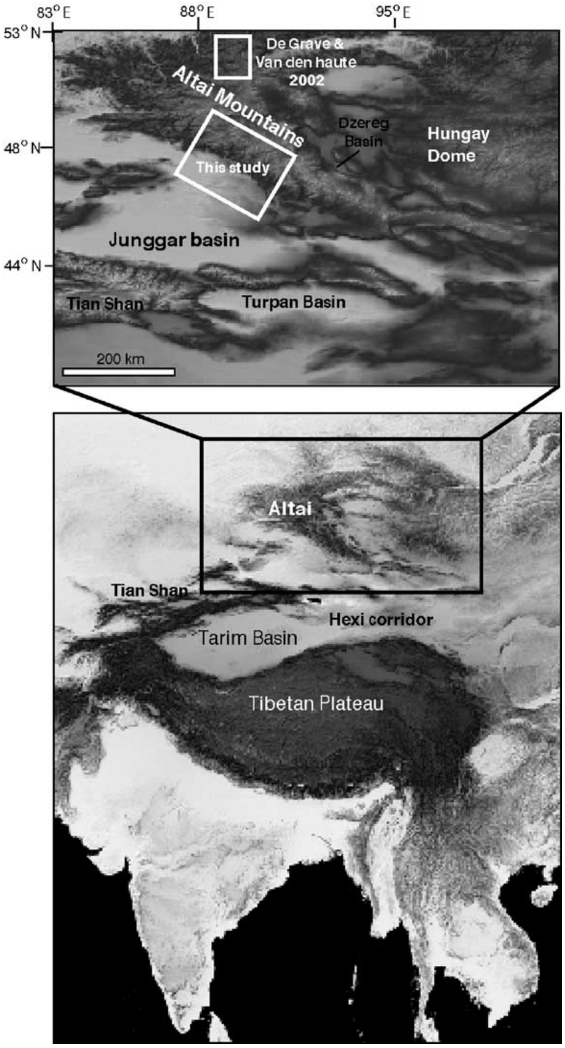

Fig. 1. Digital elevation map showing the location of the study area, previous work by DeGrave and Van den Haute (2002) and mountain belts and basins referred to in the text.

The evolution of the Altai Mountains since the late Mesozoic is also unknown. Evidence from the Russian section of the Altai Mountains to the west indicate that the mountain belt was progressively denuded throughout the Late Cretaceous and Palaeogene during a period tectonic quiescence (Dobretsov et al., 1995). Whilst to the east, closure of the Mongol-Okhotsk Ocean in the Jurassic and Early Cretaceous as the Sino-Korean continent finally joined with the Siberian Craton, may have led to significant uplift and formation of a large mountain belt. This contrasting history was investigated by DeGrave and Van den Haute (2002) applying apatite fission track analysis (AFT) to rocks from the Lake Teletskoye Region (Fig. 1) of the Altai Mountains in southern Siberia. Their results identified a Late Jurassic–Early Cretaceous cooling event consistent with uplift associated with closure of the Mongol-Okhotsk Ocean. A later phase of accelerated cooling in the Late Miocene–Pliocene was interpreted as probably related to distal effects of the India/Eurasia collision. A key question therefore is how much has the present-day topographic relief of the Altai region been influenced by far field effects (tectonic and/or climatic) arising from the India–Eurasia collision? To answer this question is beyond the scope of this study which aims to investigate rock cooling histories of a section of the Altai Mountains located in northeastern China (northern Xinjiang) between 87–89° E and 47–49°N (Fig. 1) building on the earlier smaller scale study of DeGrave and Van den Haute (2002). Only through such studies is it possible to recognize any temporal links with Himalayan orogenesis.

2. Regional geology and deformation history

The geology and deformation history of the Altai Mountains is complex (Fig. 2), and involved several phases of crustal accretion and magmatism (mostly in the Palaeozoic) defined by large NW–SE trending strike-slip fault zones. Foremost was the northward subduction of the Kazakhstan-Junggar Ocean in the Early Paleozoic (Chen et al., 1997; He et al., 1995) that resulted in magmatism and deformation that increased in intensity from the NE to SW (Dong, 2000). The Irtysh-Mayinebo zone (Fig. 2), on the southern margin of the Altai orogen, is characterized by Devonian to Carboniferous volcanic rocks considered to represent a volcanic arc associated with subduction of Junggar oceanic crust. Final closure of the Junggar oceanic basin with collision between the Kazakhstan and Siberian plates occurred by the Late Carboniferous. In the Permian the tectonic regime

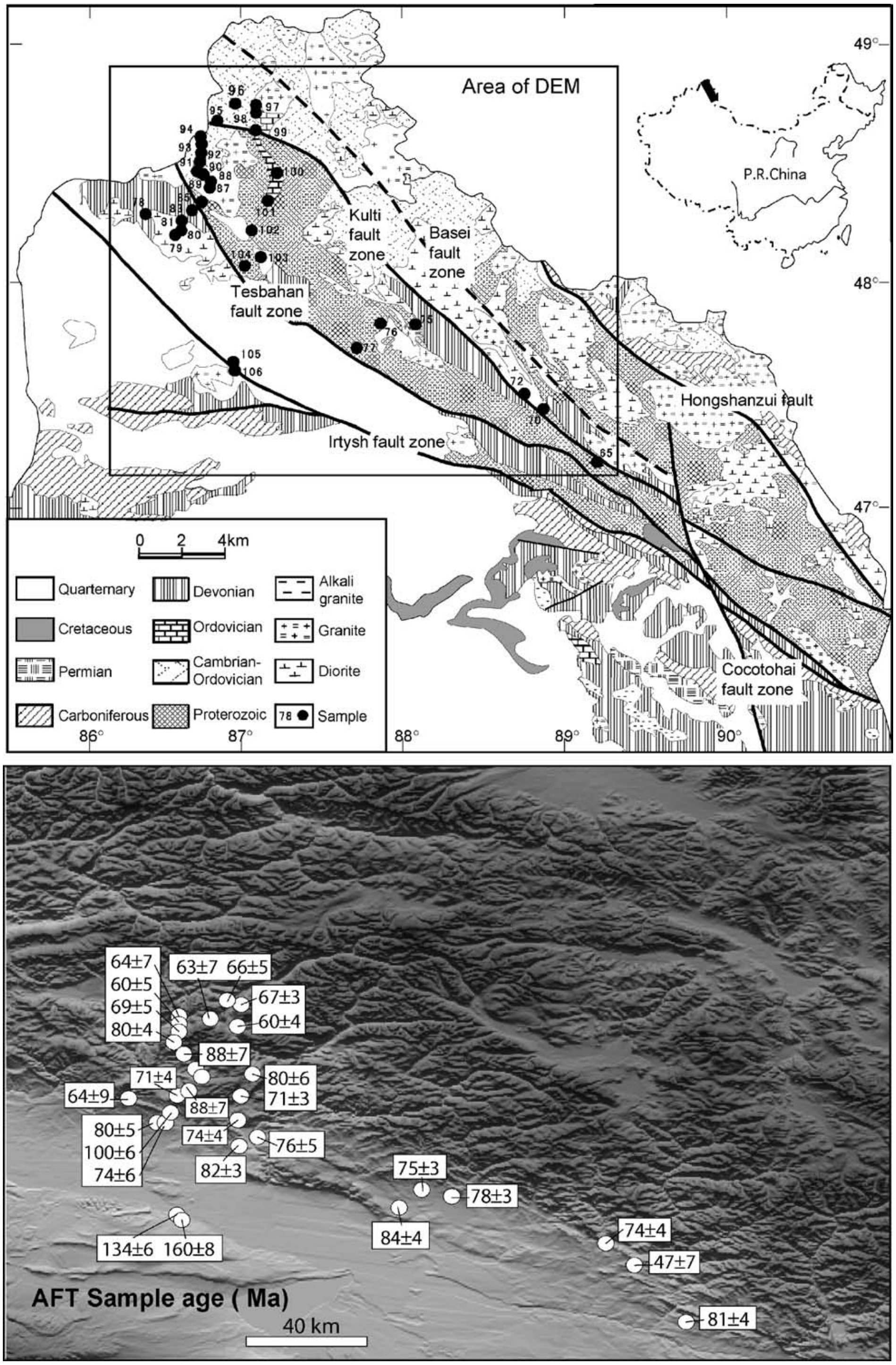

Fig. 2. Generalised geological map of the Altai region showing locations of the surface samples. The DEM shows the sample AFT ages and their location with respect to the terrain.

was predominantly collisional although Allen et al. (1995) propose a Late Permian transentional phase. With ongoing convergence the Junggar oceanic basin evolved into the Jungar intracontinental foreland basin that during the Mesozoic and Cenozoic accommodated up to 5 km of non-marine clastic sediments. Throughout the Mesozoic Junggar Basin sedimentation switched between debris flows and alluvial fans

(Wang and Chen, 2004), braided rivers and lacustrine environments as a series of discrete collision events, related to continental slithers (Qiantang and Lhasa) colliding and suturing to the Asian margin, waxed and waned. These events promoted thrusting and deformation that generated sufficient topographic relief to drive the erosion to produce large alluvial fan systems. Given that significant erosion was taking place it is unknown if the Altai region remained a mountain belt in the Mesozoic (Sjorstrom et al., 2001). Final collision related events to affect the Altai region took place in the Cenozoic as India collided with Asia to form the Himalayas and Tibetan Plateau.

The Palaeozoic subduction–accretion events formed large NW–SE trending fault zones that clearly influenced regional tectonic development. The Irtysh fault zone and dextral strike-slip zone consisting of five faults accommodated about 650 km of E–W extension. Either side of the fault zone there are clear differences in the style of magmatism, metamorphism and mineralization associated with up to 7 km of vertical displacement across the fault (Zari, 1994). Whilst these fault zones imply a long period of activity little is known about how they may have affected patterns of rock uplift and exhumation during the Mesozoic and Cenozoic. In the Junggar region Allen and Vincent (1997) report evidence for Mesozoic and Cenozoic reactivations on basement structures. The Irtysh fault zone has certainly been active since the Pleistocene (Bai, 1996). In addition the Mesozoic north–northwest striking 190 km long Cocotahai-Ertai fault zone (Fig. 2) has shown right lateral reverse slip since the Late Pleistocene, causing disruption to the drainages of the Irtysh and Ulungur rivers (Bai et al., 1996; Dong, 2000). Whilst Pleistocene reactivations are consistent with the effects of shortening taken up by Central Asia as a result of collision with India, it is unclear if such effects have a longer history. Thermochronological evidence from the Chinese Tian Shan Mountains to the south show Himalayan related Cenozoic accelerated cooling begun ~25 Ma (e.g. Sobel and Dumitru, 1997) consistent with a renewed phase of uplift. Importantly, Cenozoic rock uplift in the Tian Shan is generally <3 km and much of the present-day topography is closely associated with Mesozoic mountain building.

3. Methology

Fig. 2 shows the regional geology and sample locations. The samples were broadly collected as NNE traverses across the principal NW–SE trending fault zones from a range of rock types ranging in age from the Proterozoic to Permian. Apatite separation followed conventional crushing, heavy liquid and magnetic separation techniques. Most samples yielded sufficient apatite grains for AFT analysis. Apatite grains were mounted in epoxy resin on glass slides, ground and polished to an optical finish to expose internal grain surfaces. Spontaneous tracks were revealed by 7% HNO_3 for 40 s at 25 °C. Samples were irradiated in a well-thermalized (Cd for Au > 100) neutron flux in the 492 Swim reactor at Beijing. Muscovite was used as an external detector that after irradiation were etched in 40% HF for 20 min at 25 °C. Fission track densities in both natural and induced fission track populations were measured in air at ×1000 magnification. Only those crystals with prismatic sections parallel to the c-crystallographic axis were accepted for analysis, these crystals being of a high etching efficiency. Neutron fluence was monitored using the CN5 uranium dosimeter glass. Lengths of horizontal confined fission tracks were measured using similar conditions to those employed for age determinations. As many track lengths as possible were measured (up to ~100), for each sample. Fission track central ages (Galbraith and Laslett, 1993) were calculated using the IUGS-recommended Zeta calibration approach (Hurford and Green, 1982; Hurford, 1990). The weighted mean zeta values for apatite used in this study are 322.1 ± 3.6.

Following measurement, fission track ages and length data were modeled using the annealing model of Ketcham et al. (1999). Apatite composition was monitored using a combination of etch pit dimensions (Dpar) and absolute measurement by electron microprobe analysis using a JEOL electron microprobe, with an accelerating voltage of 15 kV, a beam current of 29 nA, and a 20 μm defocused electron beam to avoid problems associated with apatite decomposition. Most samples were shown to be flourapatites with chlorine below detection levels.

4. Fission track results

Thirty-two samples were analyzed yielding central ages between 163.0 ± 6.4 and 46.9 ± 7.2 Ma. Most ages fall between 100.4 ± 5.7 and 46.9 ± 7.2 Ma (Table 1, Fig. 2). The two exceptions, 160.5 ± 8.3 and 133.9 ± 6.0 Ma, come from the southern margin of the Altai Mountains near the Irtysh fault zone. All AFT ages are younger than the sample depositional or emplacement ages (Proterozoic through to Permian). A number of samples have χ^2 values <5%. The cause of this extra

Table 1

Sample ref	Elevation (m)	Rock type	No grains	P_s (N_s)	P_i (N_i)	$P(\chi^2)$	Central age (Ma) $\pm 1\sigma$	Mean track length (μm)	Standard deviation (μm)	No. tracks
TS106	630	Granite	29	8.062 (1864)	7.651 (1769)	0.2	160.5 ± 8.3	12.7 ± 0.2	1.7	106
TS105	511	Granite	26	10.136 (1570)	11.679 (1809)	9.7	133.9 ± 6.0	12.7 ± 0.2	1.9	104
TS104	828	Gneiss	25	4.998 (1415)	9.456 (2677)	49.7	82.3 ± 3.3	13.2 ± 0.2	1.8	107
TS103	749	Granite	25	3.128 (463)	6.318 (935)	22.6	76.0 ± 5.2	12.8 ± 0.2	2.1	100
TS102	1124	Granite	22	15.370 (976)	32.173 (2043)	12.8	74.3 ± 3.7	13.0 ± 0.2	1.6	106
TS101	1582	Gneiss	25	18.163 (2156)	39.882 (4734)	2.0	71.1 ± 2.8	13.4 ± 0.1	1.4	103
TS100	1764	Gneiss	16	6.435 (408)	12.476 (791)	23.0	79.9 ± 5.6	13.2 ± 0.2	1.8	105
TS99	1369	Sandstone	15	7.486 (376)	19.251 (967)	79.5	60.0 ± 4.1	12.7 ± 0.1	1.5	102
TS98	1494	Granite	7	14.667 (352)	31.417 (754)	5.6	75.3 ± 7.2	12.8 ± 0.4	1.7	15
TS97	1839	Granite	15	7.708 (269)	17.564 (613)	2.3	63.4 ± 6.9			
TS96	1726	Sandstone	23	11.808 (764)	27.697 (1792)	74.0	66.5 ± 3.3	12.6 ± 0.4	1.8	23
TS95	1399	Slate	17	10.486 (548)	23.859 (1249)	12.2	66.6 ± 4.8			
TS94	1486	Diorite	18	4.405 (185)	10.286 (432)	41.6	64.4 ± 6.9	13.1 ± 0.2	1.8	102
TS93	1585	Breccia	25	3.79 (364)	8.902 (855)	21.2	66.7 ± 4.8	12.6 ± 0.2	2.3	101
TS92	1321	Sandstone	10	8.089 (199)	20.976 (516)	51.6	60.2 ± 5.2	11.8 ± 0.5	1.8	15
TS91	1185	Schist	18	2.421 (266)	5.488 (603)	84.6	68.8 ± 5.3	12.9 ± 0.2	1.6	51
TS90	1030	Granite	11	25.641 (900)	45.242 (1588)	19.7	87.5 ± 4.5	13.5 ± 0.2	2.0	102
TS89	1107	Granite	28	13.501 (1905)	22.863 (3226)	74.2	91.9 ± 3.3	13.7 ± 0.2	1.7	108
TS88	1321	Granite	19	12.95 (889)	24.414 (1676)	44.6	82.4 ± 4.1	14.5 ± 0.1	1.4	103
TS87	1164	Granite	23	28.233 (1965)	53.851 (3748)	0	80.4 ± 3.8	13.5 ± 0.1	1.5	103
TS85	1433	Gneiss	7	5.493 (224)	9.711 (396)	2.8	88.0 ± 7.6			
TS83-2	1208	Gneiss	6	1.652 (33)	3.605 (72)	81.2	71.4 ± 15.1	12.6 ± 0.3	1.9	32
TS81	1164	Gneiss	11	16.222 (438)	31.444 (849)	48.0	79.9 ± 5.3	13.2 ± 0.2	1.6	101
TS80	989	Granite	25	24.607 (940)	38.455 (1469)	5.1	100.4 ± 5.7	12.9 ± 0.2	1.6	108
TS79	815	Granite	13	9.094 (293)	19.336 (623)	27.1	73.7 ± 6.4	11.3 ± 0.4	2.7	46
TS78	897	Cu-ore	10	2.669 (126)	5.699 (269)	15.1	62.4 ± 10.6	11.6 ± 0.6	2.8	22
TS77	659	Granite	23	13.663 (1369)	25.190 (2524)	95.6	84.4 ± 3.4	12.9 ± 0.2	1.6	102
TS76	699	Gneiss	16	8.092 (1582)	16.777 (3280)	9.5	75.3 ± 3.2	13.4 ± 0.2	1.6	107
TS75	951	Granite	23	15.691 (1464)	31.265 (2917)	88.5	78.2 ± 3.0	13.6 ± 0.2	1.6	104
TS72	1206	Granite	18	10.156 (716)	21.319 (1503)	9.8	74.1 ± 4.2			
TS70	1266	Granite	2	5.839 (80)	19.051 (261)	9.3	46.9 ± 7.2			
TS65	1170	Granite	24	8.092 (1667)	15.927 (3281)	0.7	80.6 ± 3.8	13.3 ± 0.1	1.5	102

ρ_s and ρ_i are fossil track density and induced track density, respectively ($\times 10^6$ tcm^{-2}). Dosimeter track density is 1.04×10^6 /cm and Nd = 2607. N_s and N_i are fossil track and induced track. $P(\chi^2)$ is probability (Galbraith, 1981).

Poissonian variation is unclear. No systematic age/compositional effects were detected. Examination of the percentage of age dispersion about the central age shows that for most samples the spread in single grain ages is not significant. This is supported by a consistency in central age between samples that both fail and pass the χ^2 test. The mean track lengths (MTL) range between 14.5 ± 0.1 and 11.3 ± 0.4 μm with standard deviations between 1.4 and 2.7μm (Fig. 3) In general the mean track lengths are moderately long (circa 13 μm) consistent with residence at low annealing temperatures (50–70 °C).

Part of the rationale for collecting samples as a traverse across the main fault zones was to see, if, over the long-term, there had been any differential block movement or, if the region has behaved more uniformly in response to regional rock uplift. In this regard the data can be considered in terms of their position relative to the faults as well as vertical position in the rock column. Fig. 4 plots AFT age for all samples with respect to elevation. The plot shows no clear relationship between age and sample elevation as would be expected from a region experiencing uniform exhumation. The two oldest samples from adjacent to the Irtysh fault (Fig. 2) occur at the lowest elevations. However, the older ages seem unrelated to the thirty samples collected further north. Is this difference due to variable levels of exhumation of the blocks either side of the fault zone? Examination of age and elevation and sample location reveals no systematic relationship. Fig. 5 plots age and elevation of samples between the Irtysh, Tesbahan and Kulti fault zone (see Fig. 2) and reinforces the view that there is no evidence for differences in exhumation between the fault zones. Overall, whilst there is some scatter within the dataset, ages and track lengths are similar and show no systematic relationship to sample position or elevation. The general similarity in AFT ages and lengths suggest a common thermal

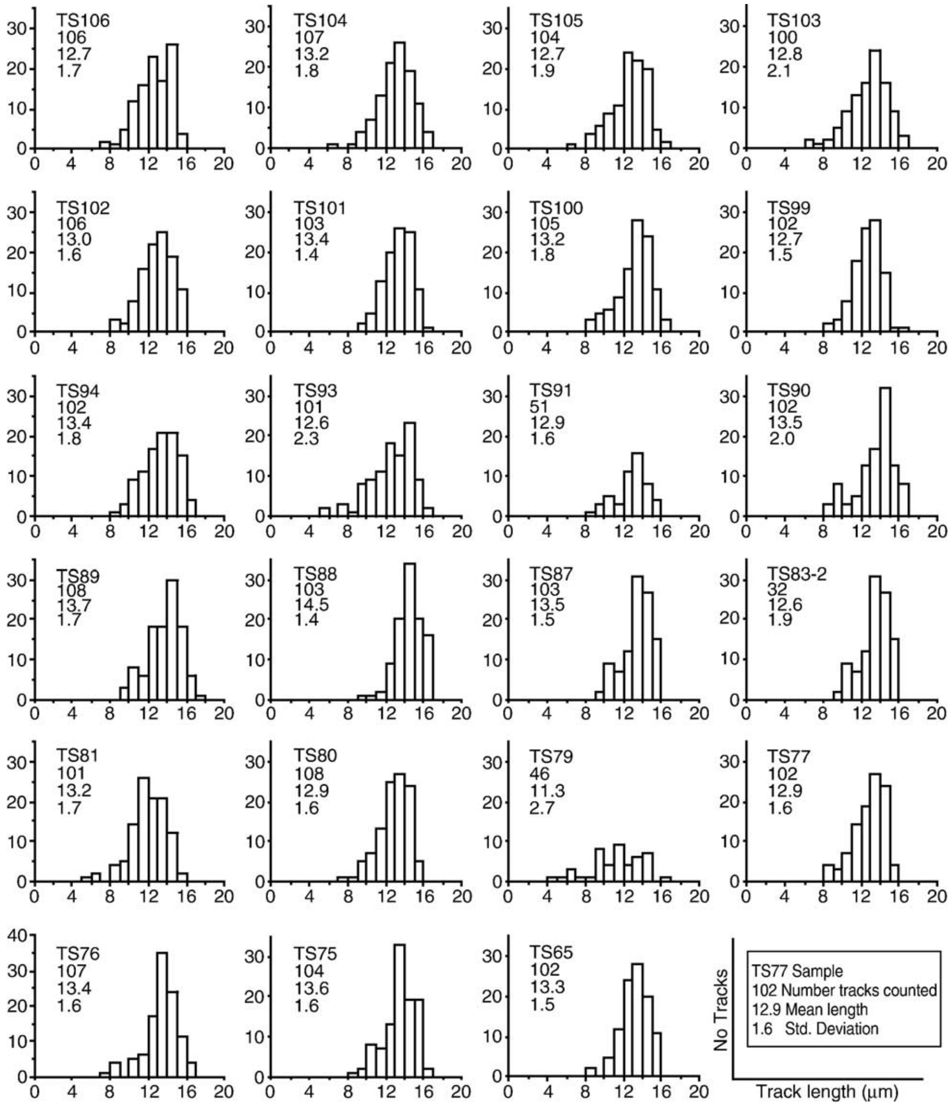

Fig. 3. Histograms of the apatite fission track length distributions measured on the samples in this study. The mean track lengths range between 14.5 ± 0.1 and 11.3 ± 0.4 μm with standard deviations between 1.4 and 2.7 μm. In general the mean track lengths are moderately long (circa 13 μm) consistent with residence at low annealing temperatures (50–70 °C).

history. Applying quantitative thermal history modeling to suitable individual sample data more rigorously tests this possibility.

5. Thermal history modeling

Based on the annealing model of Ketcham et al. (1999), thermal histories of samples that best predict the observed data were modeled using the Monte Carlo method with the AFTSolve software program (Carlson et al., 1999; Donelick et al., 1999; Ketcham et al., 1999, 2000). Only samples with sufficient numbers of measured confined tracks (>75) were used in the modeling. The inversion procedure maps the range of time–temperature paths that predict the measured data. The only constraints placed on modeling were a requirement to reach surface temperatures at the present time and to cool from temperatures higher than the relevant apatite partial annealing zone (PAZ) temperatures. In most cases the FT data were unable to constrain cooling prior to the Jurassic. Fig. 6 shows examples of modeled thermal histories. In each plot the bold line represents the best-fit history whilst the dashed lines delineate envelopes of 'good-fit' thermal history models based on the Kolmogorov–Smirnov test probability value >0.5, which is used to compare the measured fission

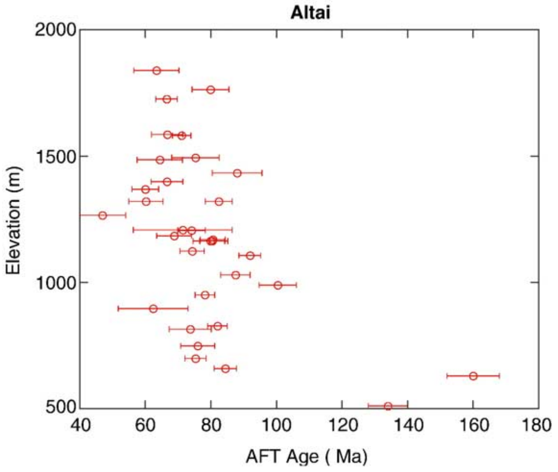

Fig. 4. Plot of AFT age and elevation for all samples analysed in this study. The data show no clear relationship between age and sample elevation as would be expected from simple exhumation of a region of low topographic relief.

track length distribution to the model predicted length distribution, and the goodness-of-fit between measured and predicted age data. For each of these statistics, a "good-fit" result corresponds to a value of 0.50 or higher.

Modeling reveals that most sample FT data can be produced by a three stage cooling history. The first stage is a requirement for rapid cooling during the Cretaceous. The onset and hence magnitude of cooling cannot be constrained by the apatite FT data, as cooling in most samples initiated at temperatures above the total annealing temperature for fission tracks in apatite (>~110–120 °C) and so it is unclear when this began. However, by the Late Cretaceous all samples had reached similar shallow crustal levels within the temperature range of ~70 ± 10 °C. Following cooling samples remained within the low temperature region of track annealing for most of the Tertiary. Any cooling over this interval was relatively minor and is consistent with a period of relative tectonic quiescence. The last stage is a Miocene increase in cooling, typically from temperatures of ~60 ± 10 °C. The timing of onset of this cooling is not precise because by this time the samples would have experienced only minor levels of annealing.

6. Discussion

The apatite fission track results and modeling show the study area experienced a three stage cooling history spanning the Late Mesozoic and Tertiary. The earliest detectable stage involved cooling that ended in the Late Cretaceous when samples reached temperatures of ~70 ± 10 °C. Whilst the FT data are unable to constrain the time of onset and magnitude of this cooling phase the average 40–50 °C of cooling seen in the modelling places a minimum on the amount of rock uplift and exhumation, estimated to between ~1.3 and 1.7 km based on global average geothermal gradients of 30 °C/km. This average value ignores complexities such as local variation in thermal conductivity associated with different sediment packages. What drove this cooling? As India drifted northwards in the late Mesozoic subduction closed small oceans such as Meso-Tethys, and continental slithers and island arcs collided in succession with the Asian margin. Each collision event would have caused compression across Asia spanning several to tens of millions of years. In terms of the Cretaceous cooling seen in the AFT results exhumation and erosion linked to collision of the Lhasa block with Asia in the Lower Cretaceous (Zanchi et al., 2000) is most the likely cause. In the Junggar Basin on the southern margin of the Altai (Fig. 1) there is clear evidence for regional compression that caused pre-Cretaceous strata to dip more steeply than Cretaceous strata. The basal unconformity in the Early Cretaceous Tugulu Group marked by a poorly sorted pebble grade breccia (Vincent and Allen, 2001) defines a time of non-deposition and formation of erosion surfaces in the basin and uplift in the alluvial sediment hinterland. Fig. 7 shows the temporal correspondence between Junggar Basin burial history and a generalized thermal history based on the modeled AFT data. Based on this evidence Cretaceous compression almost certainly extended to the Altai region to the north.

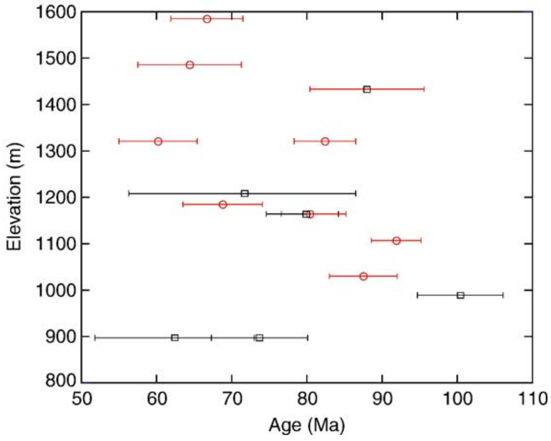

Fig. 5. Plot of sample AFT age and elevation for samples collected across blocks between the Irtysh and Tesbahan fault zones (squares) and Tesbahan and Kulti fault zone (circles). The plot shows no evidence for different exhumation histories between each block.

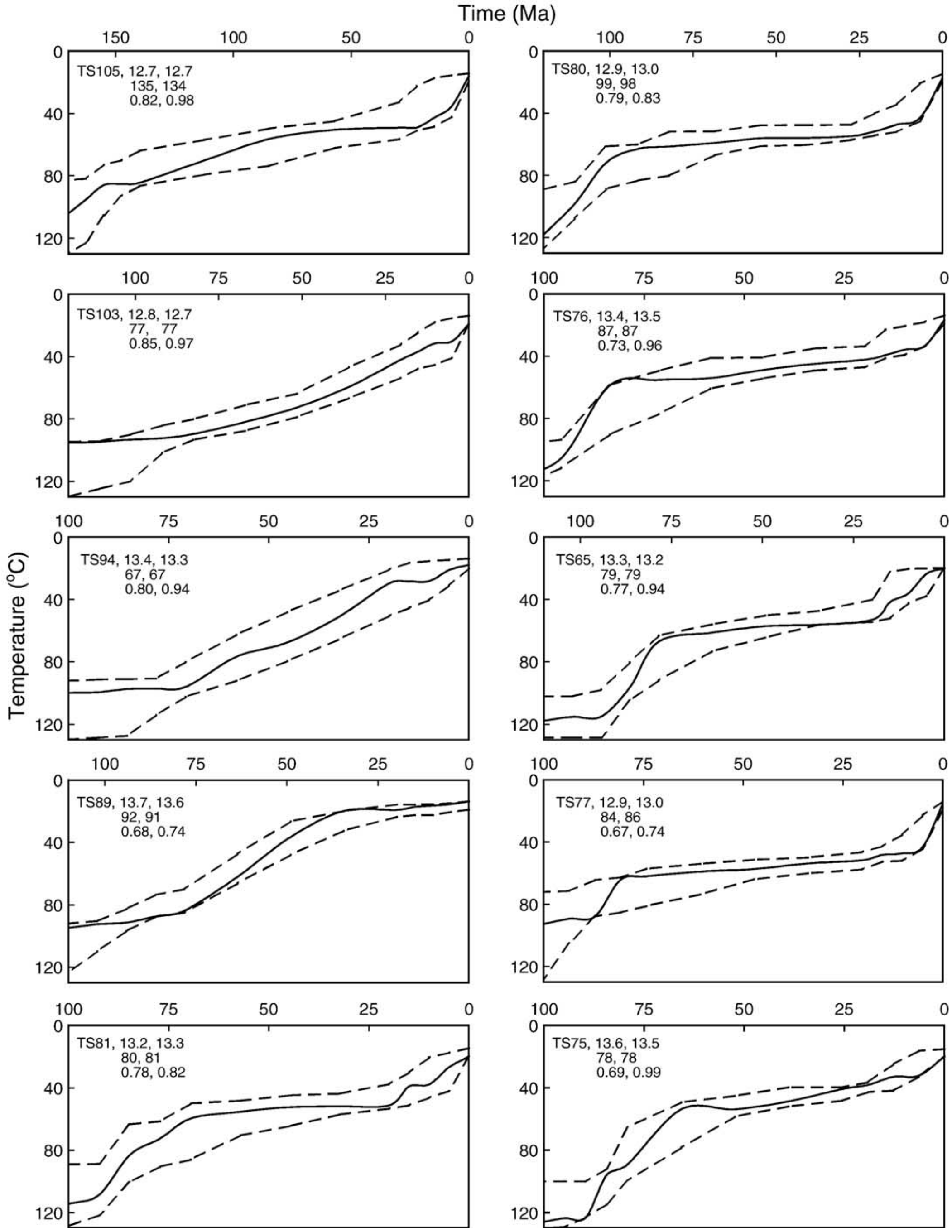

Fig. 6. Time–temperature histories of samples from the Altai Mountains calculated by inverse modeling observed apatite fission track parameters, based on the annealing model of Ketcham et al. (1999). Field between dashed lines is the goodness-of-fit result predicted by the model, and the solid line is the best-fit result. The *X*- and *Y*-coordinate reflect the fission track age (Ma) and the temperature (°C), respectively. At the top left of every plot are given the sample number, measured and model predicted track length, measured and modeled pooled age, and Kolmogorov–Smirnov test, which is used to determine similarity between measured and predicted AFT age and length parameters.

The second stage in the AFT modeled cooling history of the Altai indicates a period of relative tectonic quiescence with samples remaining throughout the Paleogene at more or less the same crustal depth first reached in the Late Cretaceous. Any Paleogene cooling was thus minor and is consistent with little if any erosion. A similar pattern is seen in the Junggar Basin where hardly any subsidence occurred

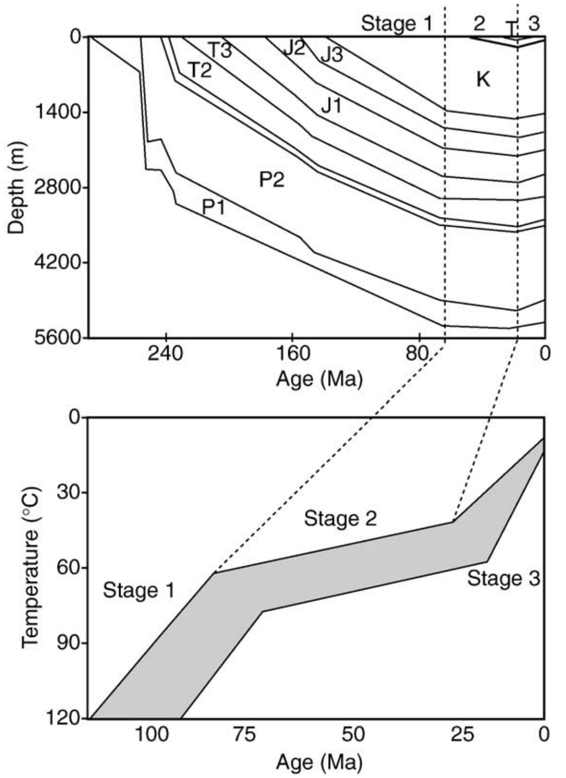

Fig. 7. Comparison of a generalised summary thermal history based on the modeled AFT data and burial history of the Junngar Basin (Fig. 1), after Wang et al., 2001.

throughout this time and any sedimentation was mostly lacustrine. An exception is in southern parts of the Junggar Basin and the north Tarim Basin (Fig. 1) where the Late Cretaceous is marked by influx of course prograding conglomerates consistent with some local uplift along parts of the basins margins. Timing is coincident with collision and onset of subduction of the Kohistan-Ladakh Arc terranes (Hendrix et al., 1992). However, there is no clear evidence within the AFT data that such deformation extended to the Altai region.

The lack of significant Late Cretaceous–Palaeogene sedimentation in the Junggar Basin is compatible with a subdued low-relief hinterland implying that any significant topographic relief associated with Mesozoic accretion–subduction had effectively been leveled off by this time. This interpretation is consistent with observations made in the northern Altai (South Siberia) where there are remnants of a Late Mesozoic erosional peneplain (DeGrave and Van den Haute, 2002). Evidence for this erosion surface can be found across a large area. In the Hangay region of central Mongolia (Fig. 1) planation surfaces can be found over an area of 200,000 km^2. Further to the east in the Hexi Corridor (a Cenozoic foreland basin formed at the north-eastern margin of the Qinhai-Tibet Plateau, Fig. 1), Late Cretaceous to Eocene sediments are missing due to erosion (Li and Yang, 1998).

The third stage in the cooling history of the Altai involves accelerated cooling that began in the Miocene and ended with sample exhumation. This final stage of cooling (less than ~70 °C) occurs over temperatures at the limit of resolution by the FT method and could be considered an artifact of the modeling. However there is significant regional evidence to support the existence of this cooling stage. In the Altai region the Late Cretaceous–Eocene erosion surfaces are today found at elevations >3500 m (Cunningham, 2001) indicating that since the Paleogene there has been significant regional surface uplift. The extent of this uplift was far reaching. In the Tian Shan Mountains to the southwest (Fig. 1) tectonism and surface uplift started around 25–20 Ma and is considered linked to a change from extrusion-dominated to crustal-thickening-dominated strain accommodation in the Himalaya (Bullen et al., 2001; Sobel and Dumitru, 1997). An Oligocene unconformity in basins along the eastern margin of the Altai such as the Dzereg and Dariv basins marks the onset of deformation in the Mongolian Altai (Howard et al., 2003; Cunningham, 2001). Here fluvial and debris dominated sediment record initial uplift of the basins flanking ranges during the Miocene. Sedimentation also becomes increasingly conglomeratic through the Pliocene and Pleistocene (Howard et al., 2003). In both the Tarim and Junggar Basins the bulk of Cenozoic deposition has occurred since the early Neogene, i.e. ~23 Ma (Wang, 1995; Zhang, 1993). In the more distant Hexi foreland basin Cenozoic sedimentation (fluvio-lacustrine intercalated with volcanic rocks) only increased after the Oligocene (Jolivet et al., 2001; Li and Yang, 1998). Based on this widespread regional evidence we consider the post Oligocene acceleration in cooling recorded in the AFT models to be real. The cause of this cooling is considered linked to a phase of renewed uplift most likely due to propagation of crustal thickening dominated strain associated with continued growth of the Himalaya-Tibet.

At the outset of this study we asked whether there had been any differential movement across the main basement fault bounded blocks. The available evidence shows no systematic relationship between FT age and length and sample location. Similarly there is no apparent systematic difference in the modeled thermal histories linked to these structures. Reactivations would only be detected if there were differential vertical motion and erosion across the fault blocks. The apatite FT data thus limit any movement to the small scale.

7. Concluding remarks

Based on modeled AFT data this study has identified a 3 stage cooling history that affected the Altai region. This cooling is inferred to record changes in rock uplift and erosion in response to regional deformation events. This inference is supported by sedimentation history of adjacent (and more distal) sedimentary basins that mirrors the changes in AFT modeled cooling rate. Together the Junggar Basin sedimentation history and modeled AFTdata show the Altai region was reduced to a low relief peneplain by the late Mesozoic and early Tertiary. This means that the present-day topography and relief of the Altai Mountains are a relatively recent (Neogene) development. It seems likely, based on the AFT results and regional evidence that Altai Mountain topography only started to develop from the Miocene onwards as a direct result of the far field effects of the Himalayan collision principally driven by overthickened crust. Such effects have been observed in the Tian Shan Mountains to the south where the topography is also considered to be in the Late Cenozoic.

Acknowledgement

This work was supported by the National Basic Research Priorities Program (No. 2001CB409804) and the Nature Science Foundation of China (No. 10175076, 40072068 and 10475093). The authors thank Profs. Gao Jun, Shu Liangshu and Zhang Zhicheng for discussion and good suggestions. Mrs. Zhu Bingyu and Wang Yu kindly assisted us in obtaining geological data and “field work”. We are grateful to the support from all members, especially Prof. Wang Shicheng, of the Fission Track Group, IHEP. We would like to acknowledge Prof. A.G.W. Gleadow, Drs. B.P. Kohn, A. Raza and Prof. Rod Brown for their help with the fission track technique in the past.

References

Allen, M.B., Vincent, S.J., 1997. Fault reactivation in the Junggar region, northwest China: the role of basement structures during Mesozoic–Cenozoic compression. J. Geol. Soc. Lond. 154, 151–155.

Allen, M.B., Sengör, A.M.C., Natalin, B.A., 1995. Junggar, Turfan and Alakol basins as Late Permain to Early Triassic extensional structures in a sinistral shear zone in the Altaid orogenic collage, Central Asia. J. Geol. Soc. Lond. 151, 327–338.

Bai, M., 1996. Irtysh active fault zone. Xinjiang Geol. 14, 127–134 (in Chinese with English abstract).

Bai, M., Luo, F., Yin, G., Xiang, Z., Sheng, J., Shi, S., Ding, D., Guo, H., Ruan, C., 1996. Kokotakay–Ertai active fault zone in Xinjiang. Inland Earthq. 10, 319–328 (in Chinese with English abstract).

Bullen, M.E., Burbank, D.W., Garver, J., Abdrakhmatov, K.Y., 2001. Late Cenozoic tectonic evolution of the northwestern Tien Shan: new age estimates for the initiation of mountain building. Geol. Soc. Amer. Bull. 113, 1544–1559.

Carlson, M.D., Donelick, R.A., Ketcham, R.A., 1999. Variability of apatite fission-track annealing kinetics: experimental results. Am. Mineral. 84, 1213–1223.

Chen, Z., Cheng, S., Liang, Y., Xu, X., 1997. Opening–closing tectonics and mineralization in Xinjiang. Xinjiang Science Technology and Hygiene Publishing House (K), Urumqi, China, 111-172.

Cunningham, W.D., 2001. Cenozoic normal faulting and regional doming in the southern Hangay region, Central Mongolia: implications for the origin of the Baikal rift province. Tectonophysics 331, 389–411.

DeGrave, J., Van den Haute, P., 2002. Denudation and cooling of the Lake Teletskoye Region in the Altai Mountains (South Siberia) as revealed by apatite fission-track thermochronology. Tectonophysics 349, 145–159.

Dobretsov, N.L., Berzin, N.A., Buslov, M.M., 1995. Opening and tectonic evolution of the Palaeo-Asian Ocean. Int. Geol. Rev. 37, 335–360.

Donelick, R.A., Ketcham, R.A., Carlson, W.D., 1999. Variability of apatite fission-track annealing kinetics: crystallographic orientation effects. Am. Mineral. 84, 1224–1234.

Dong, Y., 2000. Distribution of gold deposits resulted to fault structures in Altay, Xinjiang. Volcanol. Miner. Resour. 2, 41–46 (in Chinese with English abstract).

Galbraith, R.F., 1981. On statistical models for fission track counts. Math. Geol. 13, 971–988.

Galbraith, R.F., Laslett, G.M., 1993. Statistical models for mixed fission track ages. Nucl. Tracks Radiat. Meas. 21, 459–470.

He, G., Liu, D., Li, M., Tang, Y., Zhou, R., 1995. The five-stage model of crustal evolution and metallogenic series of chief orogenic belts in Xinjiang. Xinjiang Geol. 13, 1–97.

Hendrix, M.S., Graham, S.A., Carroll, A.R., Sobel, E.R., McKnight, C.L., Schulein, B.J., Wang, Z., 1992. Sedimentary record and climatic implications of recurrent deformation in the Tian Shan: evidence from Mesozoic strata of the north Tarim, south Junggar and Turpan basins, northwest China. Geol. Soc. Amer. Bull. 104, 53–79.

Howard, J.P., Cunningham, W.D., Davies, S.J., Dijkstra, A.H., Badarch, G., 2003. The stratigraphic and structural evolution of the Dzereg Basin, Western Mongolia: clastic sedimentation, fault inversion and basin destruction in an intracontinental transpressional setting. Basin Res. 15, 45–72.

Hurford, A.J., 1990. Standardization of fission track dating calibration: recommendation by the fission-track working group of the I.U.G.S. Subcommission on Geochronology. Chem. Geol. 80, 171–178.

Hurford, A.J., Green, P.F., 1982. A users' guide to fission-track dating calibration. Earth Planet. Sci. Lett. 59, 343–354.

Jolivet, M., Brunel, M., Seward, D., Xu, Z., Yang, J., Roger, F., Tapponnier, P., Malavieille, J., Arnaud, N., Wu, C., 2001. Mesozoic and Cenozoic tectonics of the northern edge of the Tibetan plateau: fission-track constraints. Tectonophysics 343, 111–134.

Ketcham, R.A., Donelick, R.A., Carlson, W.D., 1999. Variability of apatite fission-track annealing kinetics: III. Extrapolation to geological time scales. Am. Mineral. 84, 1235–1255.

Ketcham, R.A., Donelick, R.A., Donelick, M.B., 2000. AFTSolve: a program for multi-kinetic modeling of apatite fission-track data. Geol. Mater. Res. 2, 1–32.

Li, Y., Yang, J., 1998. Tectonic geomorphology in the Hexi Corridor, north-west China. Basin Res. 10, 345–352.

Sjorstrom, D.J., Hendrix, M.S., Badamgarav, D., Graham, S.A., Nelson, B.K., 2001. Sedimentology and provenance of Mesozoic nonmarine strata in western Mongolia: a record of intracontinental deformation. In: Hendrix, M.S., Davis, G.A. (Eds.), Palaeozoic and Mesozoic Tectonic Evolution of Central and Eastern Asia: from Continental Assembly to Intracontinental Deformation, Geol. Soc. Am. Memoir, vol. 194, pp. 361–388.

Sobel, E.R., Dumitru, T.A., 1997. Thrusting and exhumation around the margins of the western Tarim basin during Indo-Eurasian collision. J. Geophys. Res. 102, 5043–5063.

Vincent, S.J., Allen, M.B., 2001. Sedimentary record of Mesozoic intracontinental deformation in the eastern Junggar Basin, northwest China: response to orogeny at the Asian margin. In: Hendrix, M.S., Davis, G.A. (Eds.), Palaeozoic and Mesozoic Tectonic Evolution of Central and Eastern Asia: from Continental Assembly to Intracontinental Deformation, Geol. Soc. Am. Memoir, vol. 194, pp. 341–360.

Wang, Q., 1995. Xinjiang oil and gas province: Tarim, Turpan-Hami and other main basins: petrol. Geol. China 15, 660 pp. (in Chinese).

Wang, Y., Cheng, S., 2001. Xinjiang crust evolution and mineralization. Chin. J. Geol. 36, 129–143.

Wang, W., Chen, Y., 2004. Tectonic evolution and petroleum systems in the Junggar Basin. Acta Geol. Sin. 78, 667–675.

Wang, S., He, L., Wang, J., 2001. Thermal regime and petroleum systems in Junggar Basin, northwest China. Phys. Earth Planet. Inter. 126, 237–248.

Zanchi, A., Poli, S., Fumagalli, P., Gaetani, M., 2000. Mantle exhumation along the Tirich Mir Fault Zone, NW Pakistan: pre-Mid Cretaceous accretion of the Karakoram Terrane to the Asian margin. In: Khan, M.A., Trelaor, P.J., Searle, M.P., Jan, M.Q. (Eds.), Tectonics of the Nanga Parbat Syntaxis and the Western Himalaya, Geol. Soc. London, Spec. Pub., vol. 170, pp. 237–252.

Zari, M., 1994. Distribution and geological characteristics of the main fracture structures in Xinjiang. J. Xinjiang Inst. Technol. 15, 188–194 (in Chinese with English abstract).

Zhang, G., 1993. Xinjiang oil and gas province—1. Junggar Basin: petrol. Geol. China 15, 390 pp. (in Chinese).